PHYSICAL REVIEW B VOLUME 7, NUMBER 2 15 JANUARY 1973

# Electronic Structure of Calcium as a Function of the Lattice Constant

Joseph W. McCaffrey
*Naval Research Laboratory, Washington, D. C.* 20390
and
James R. Anderson*
*University of Maryland, College Park, Maryland* 20740
and
Dimitrios A. Papaconstantopoulos†
*George Mason University, Fairfax, Virginia* 22030
(Received 21 July 1972)

Energy bands, Fermi surfaces, and densities of states of calcium as a function of lattice constant have been calculated self-consistently by the augmented-plane-wave method. A comparison is made with other band calculations and photoemission and de Haas–van Alphen experiments. The calculation showed that calcium changes from a normal metal to a semimetal and back to a normal metal with decreasing lattice constant in agreement with high-pressure experiments.

## I. INTRODUCTION

In an earlier communication,[1] which is here called I, it was shown on the basis of a self-consistent augmented-plane-wave (APW) energy-band calculation that calcium changes from a metal to a semimetal and back to a metal as a function of decreasing lattice constant, in good agreement with high-pressure experiments.[2–4] In this paper we report in greater detail the energy bands, Fermi surface, and density of states of Ca as a function of lattice constant. Subsequent to I there have appeared several[5–9] other calculations of the energy bands of Ca at normal lattice spacing and a comparison will be made to these results. In addition, comparison will be made to very recent photoemission results.[10]

## II. DETAILS OF CALCULATION

Since the APW method has been the subject of several reviews[11–13] it will not be treated in great detail here. The initial one-electron potentials were constructed from solutions to Poisson's equation with charge densities ($4s^2$ configuration) obtained by a superposition to fifth neighbors of the Herman–Skillman[14] free-atom charge densities using the Löwdin $\alpha$ expansion.[15] Subsequent potentials were constructed from the calculated conduction-electron-band ($4s$) charge density, plus the core. In addition, at reduced lattice constant it was necessary to include the calculated $3p$ core bands in the self-consistency cycle. For example, for a reduced lattice constant $a/a_0 = 0.9$ (where $a_0 = 5.5844$ Å[16]) it was observed that retaining the Herman–Skillman $3p$ charge densities yielded eigenvalues differing by ~ 0.02 Ry from the present result. Another indication of the need for inclusion of the $3p$ bands in the self-consistency cycle is the pressure broadening of these bands; at normal pressure the $3p$ width ($\Gamma_{15} - L_2'$) is 0.014 Ry, while at $a/a_0 = 0.7$ this width has increased to about 0.35 Ry (see Fig. 1 of I). A somewhat surprising result is that the separation between the top of the $3p$ bands and the bottom of the conduction band $\Gamma_{15}(3p)$-$\Gamma_1(4s)$, decreases by less than 15% between $a/a_0 = 1$ and $a/a_0 = 0.7$.

The charge densities were calculated on a weighted mesh of six points ($\Gamma, \Delta, X, \Sigma, W, L$) in $\frac{1}{48}$ of the Brillouin zone. Six points were judged to be sufficient since it was noted that halving the Brillouin-zone mesh gave results which differed by only ~ 0.004 Ry from the results of the large mesh.

At normal lattice spacing the energy bands were calculated with two approximations to the exchange potential, full Slater ($\alpha = 1$) exchange,[17] and the Gaspar–Kohn–Sham[18] (GKS, $\alpha = \frac{2}{3}$) exchange. The major effect of exchange is to modify the band widths while leaving the band ordering relatively unchanged. This is a well-known effect in transition metals.[13] Two values for the occupied-conduction-band width obtained from soft-x-ray measurements have been reported, 0.22 (Ref. 19) and 0.5 Ry.[20] Since the occupied band width was found to be 0.15 and 0.3 Ry for Slater and GKS exchange, respectively, the GKS form of the exchange potential, which gives a width bracketed by the two x-ray experiments, was used for the reduced-lattice-spacing calculations.

The convergence of selected energy levels, measured from $\Gamma_1$, for $a/a_0 = 0.9$ is shown in Fig. 1. It can be seen that the convergence error is less than the one introduced by sampling the charge density at only six points. Slower convergence was

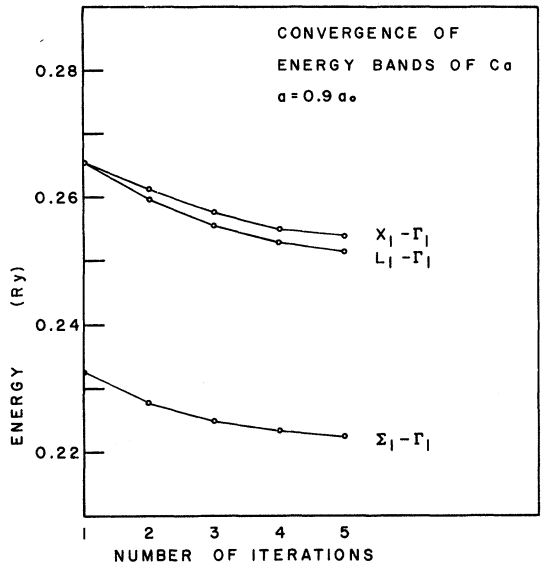


FIG. 1. Convergence of selected APW energy bands of Ca for a reduced lattice spacing of $a/a_0 = 0.9$.

observed as the lattice constant was reduced. For example, at normal lattice constant, convergent results differed from first-iteration results by ~ 0.01 Ry while for a reduced lattice constant of 0.7 the differences were ~ 0.07 Ry.

For both normal and reduced lattice spacings we have also carried out a radial integration of the self-consistent charge densities inside the muffin-tin sphere in order to obtain the angular momentum components of the band state charge. These results for six symmetry states as well as the total charge outside the muffin-tin, are given in the Appendix.

## III. BAND STRUCTURE

### A. Band Structure at Normal Lattice Spacing: Comparison with Experiment

The energy bands of calcium at normal lattice spacing are shown in Figs. 2 and 3. In addition to the earlier mentioned soft-x-ray experiments, recent photoemission measurements by Kress and Lapeyre[10] also probe relevant band widths. If we take $E_F - E(X_1)$ to be a measure of the occupied $d$-like states, then

$$E_F - E(X_1) = 0.035 \text{ Ry} = 0.48 \text{ eV},$$

which can be compared with the value of approximately 0.5 eV determined from photoemission. (Kress and Lapeyre estimated their energy resolution to be 0.2 eV.) Moreover, taking $E(X_5) - E(X_1)$ to be a measure of the total width of the $d$ band, we find

$$E(X_5) - E(X_1) = 0.469 \text{ Ry} = 6.4 \text{ eV},$$

which is also in good agreement with their measured width of 6 eV.

### B. Band Structure at Normal Lattice Spacing: Comparison with Other Calculations

In Table I we compare the results of the present calculation at normal lattice spacing with the re-

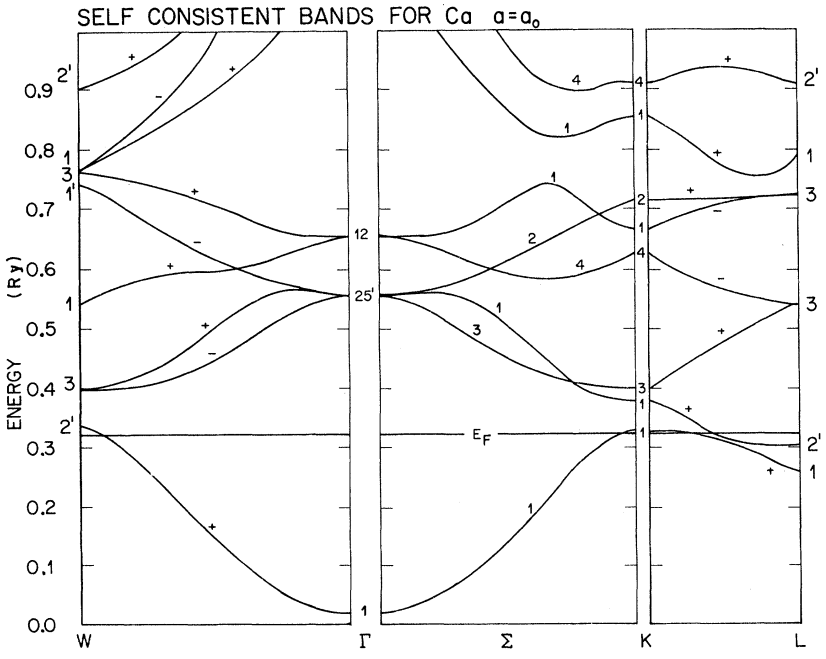


FIG. 2. Energy bands of Ca at normal lattice spacing along the $W$-$\Gamma$-$K$-$L$ symmetry directions.

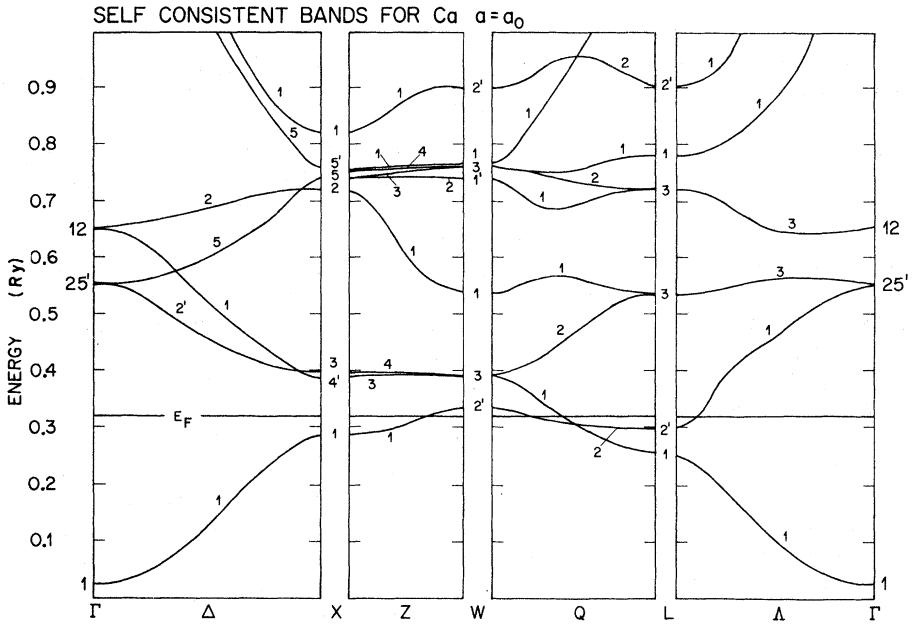


FIG. 3. Energy bands of Ca at normal lattice spacing along the $\Gamma$-$X$-$W$-$L$-$\Gamma$ symmetry directions.

sults of other recent calculations. It is useful to divide these calculations into three groups: Group 1 contains the present work and that of Dreesen and Pyenson[5] and Ross and Johnson[7]; group 2 contains the calculation of Vasvari *et al.*[21] and Chatterjee and Chakraborti[6]; and group 3 is the calculation of Altmann *et al.*[9] and Chatterjee and Chakraborti.[8]

The three calculations of group 1 are all self-consistent. Dreesen and Pyenson have used the Korringa–Kohn–Rostoker[22] (KKR) method, whereas Ross and Johnson have used the APW method. The major difference among these calculations is the treatment of exchange; Dreesen and Pyenson have used the energy-dependent Liberman[23] exchange, whereas Ross and Johnson have used the exchange factor $\alpha = 0.716$ found by Kmetko[24] to be

TABLE I. Comparison of various energy-band calculations for Ca at normal lattice spacing.

| State | Present work $\alpha=\frac{2}{3}$ | SC KKR[a] | SC APW[b] $\alpha=0.716$ | Pseudo-potential[c] | OPW[d] | Cellular[e] $\alpha=0.4$ | Quantum defect[f] |
|---|---|---|---|---|---|---|---|
| $\Gamma_1(s)$ | 0.0 | 0.0 | 0.0 | 0.0 | 0.0 | 0.0 | 0.0 |
| $\Gamma_{25}'(d)$ | 0.5300 | 0.4819 | ••• | 0.9047 | 0.7621 | 0.600 | 0.5246 |
| $X_1(s,d)$ | 0.2612 | 0.2532 | 0.2494 | 0.2966 | 0.2846 | ••• | 0.2548 |
| $X_4'(p)$ | 0.3730 | 0.3701 | ••• | 0.3586 | 0.3681 | ••• | 0.3714 |
| $X_3(d)$ | 0.3733 | 0.3496 | 0.3363 | 0.4791 | 0.4715 | ••• | 0.3769 |
| $K_1(s,p)$ | 0.2975 | 0.2885 | 0.2848 | 0.3362 | 0.3409 | 0.308 | 0.2842 |
| $K_1(s,p)$ | 0.3498 | 0.3336 | 0.3240 | 0.3939 | 0.4094 | 0.374 | 0.3547 |
| $K_3(p,d)$ | 0.3716 | 0.3625 | ••• | 0.3793 | 0.3561 | 0.397 | 0.3704 |
| $W_2'(p,d)$ | 0.3102 | 0.3003 | 0.2952 | 0.3638 | 0.3302 | 0.321 | 0.2965 |
| $W_3(p,d)$ | 0.3687 | 0.3548 | 0.3460 | 0.3958 | 0.3433 | 0.395 | 0.3675 |
| $W_1(s,d)$ | 0.5117 | ••• | ••• | 0.5433 | ••• | ••• | 0.5188 |
| $L_1(s,d)$ | 0.2353 | 0.2284 | 0.2231 | 0.2448 | 0.2846 | 0.248 | 0.2457 |
| $L_2'(p)$ | 0.2778 | 0.2761 | 0.2766 | 0.2621 | 0.2675 | 0.293 | 0.2572 |
| $E_F$ | 0.2960 | 0.2918 | ••• | 0.3386 | 0.331 | 0.308 | 0.31 |

[a]Reference 5. [b]Reference 7. [c]Reference 21. [d]Reference 6. [e]Reference 9. [f]Reference 8.

optimum for the Ca atom. It should be pointed out that although $\alpha = 0.716$ has been found to be optimum for the free atom there is no assurance that this is the best value for solid Ca. From the eigenvalues $E$ in Table I, it can be seen that, as expected,[13] the following inequality is satisfied:

$$E(\text{APW}, \alpha = \tfrac{2}{3}) > E(\text{APW}, \alpha = 0.716).$$

The KKR values fall between the two APW calculations except for the state $L_2'$. The differences in these calculations can be attributed to the different exchange potentials used. (We also note that Dreesen and Pyenson show a crossing of the two lowest bands between $K$ and $L$ which is forbidden by symmetry.)

We have associated into group 2 the orthogonalized-plane-wave (OPW) calculation of Chatterjee and Chakraborti and the non-local-model-potential calculation of Vasvari and Heine. Both these methods treat $d$-like bands poorly compared to the KKR and APW approaches (see for example the $\Gamma_{25}'$ and $X_3$ states, Table I). The poor treatment of the $d$-like states can be understood from the pseudopotential approximation, since there is no $d$ orthogonalization term (i.e., no occupied $d$ core states) to subtract from the core potential. This lack of cancellation greatly decreases the convergence rate of these methods for $d$-like bands. However, for the $s$- and $p$-like states there is generally qualitative agreement between the calculations of this group and those of group 1.

The calculations of group 3, the cellular method of Altmann *et al.*, and the quantum-defect method of Chatterjee and Chakraborti use techniques which have proved successful for the monovalent metals but have not had great success outside this family of elements. Altmann *et al.* have chosen the *unusual* value of $\alpha = 0.4$ for the exchange multiplier. Indeed their calculation yields metallic behavior only for $0.2 < \alpha < 0.75$. Their exchange factor $\alpha = 0.4$ was chosen in an *ad hoc* manner by maximizing the energy differences

$$\begin{aligned} \Delta K &= E(K_1) - E(L_2'), \\ \Delta W &= E(W_2') - E(L_2'). \end{aligned} \tag{1}$$

The values $\Delta K = 0.015$ Ry and $\Delta W = 0.028$ Ry found by Altmann *et al.* are comparable to the present work (Table I). However, for equivalent treatments of exchange the results of Altmann *et al.* are in disagreement with the calculations of groups 1 and 2. The quantum-defect method calculation gives results which are in good agreement with ours. However, this may not be significant since the details of the treatment of exchange have not been specified. In addition, because symmetry was not considered, the crossing between $W$ and $L$ was not found. The occurrence of this crossing is important because it shows that calcium will become a semimetal and not a semiconductor at reduced lattice spacings.

### C. Band Structure at Reduced Lattice Spacing

The energy bands of Ca for reduced lattice constants of 0.9, 0.8, and 0.7 are given in the Appendix; however, the important features are summarized in Figs. 4 and 5. At normal lattice spacing $\Delta W$ is positive and since there is an overlap of the first and second band, Ca has normal metallic behavior. From Fig. 4 we note that this overlap vanishes at $a/a_0 = 0.93$ ($P \sim 50$ kbar), where

$$E_F = E(W_2') = E(L_2').$$

Between $a/a_0 = 0.93$ and $a/a_0 = 0.8$, except for an accidental degeneracy along the line $L$ - $W$, there is no overlap of the first and second bands, and hence Ca will show semimetallic behavior. At a reduced lattice spacing of 0.8 ($P \sim 400$ kbar) the $d$-like state $X_3$ crosses the Fermi energy (Fig. 4) and there is a return to the metallic state. Thus calcium transforms from a metallic to a semi-

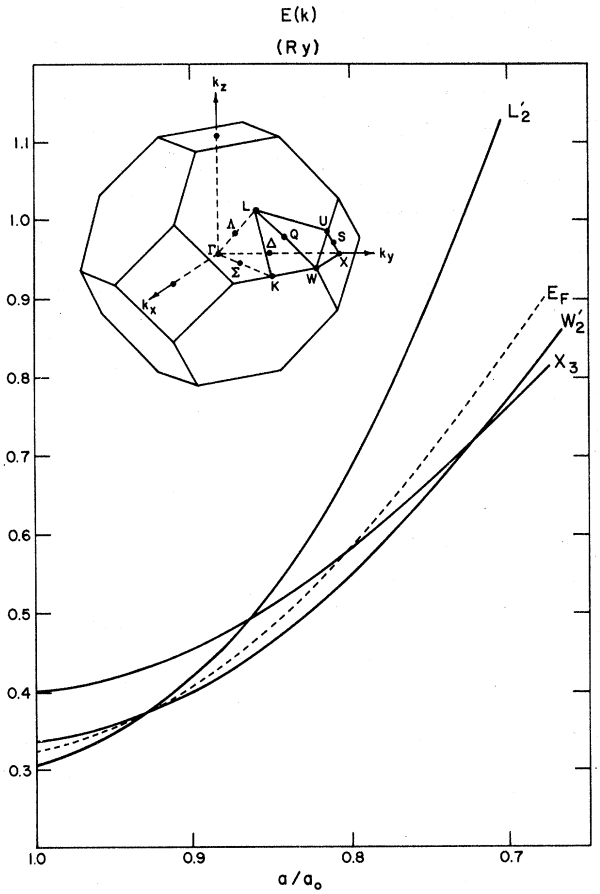


FIG. 4. Variation of the Fermi energy and the energy bands at several symmetry points with lattice constant. For each lattice constant the zero of energy is taken to be the corresponding muffin-tin constant.

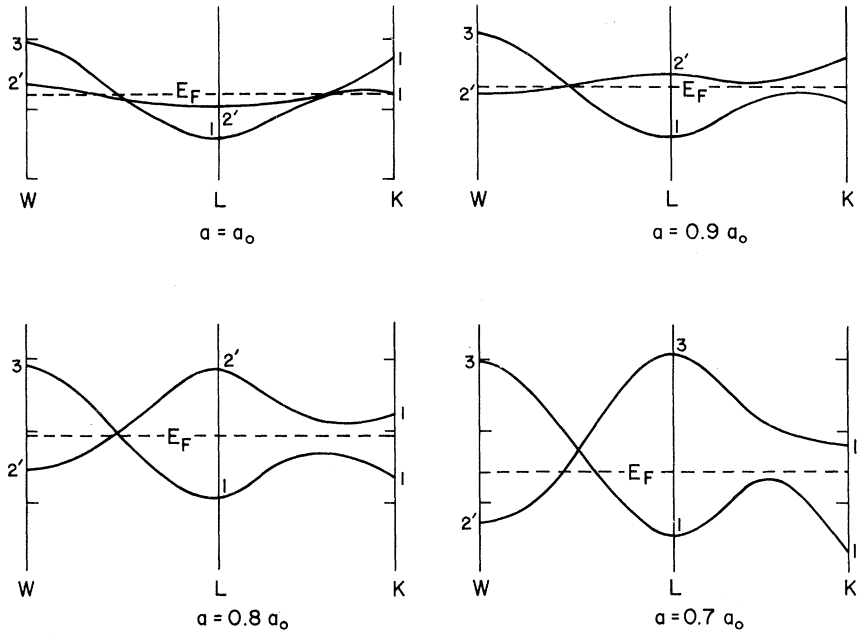


FIG. 5. Variation with lattice constant of the two lowest energy bands along the $W$-$L$-$K$ symmetry directions.

metallic and back to a metallic system as a function of pressure in agreement with high-pressure and shock-wave experiments,[2-4] as shown in I. This is an example of an electronic transition.

In ytterbium, whose band structure is similar to Ca, the accidental degeneracy along $L$ to $W$ is removed by spin-orbit coupling[25] and as expected pressure-induced metal-semiconductor transitions have been observed.[26,27]

It is possible to calculate the number of $d$ electrons inside the muffin tin as a function of lattice constant from the $Q_d$'s presented in Table III. In I, a sharp increase of the number of $d$ electrons was found at $a/a_0 \approx \frac{3}{4}$, in agreement with the shock-wave experiments of Bakanov and Dudoladov.[3]

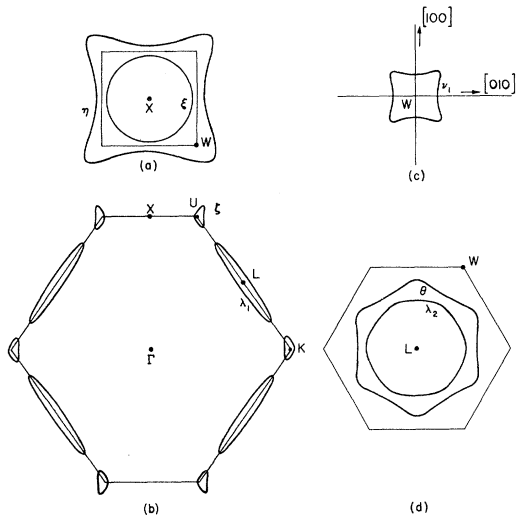


FIG. 6. Cross sections of the Fermi surface of Ca at normal lattice constant.

## IV. FERMI SURFACE AT NORMAL AND REDUCED LATTICE SPACING

In Fig. 6 we show selected cross sections of the Fermi surface obtained by graphical interpolation of the APW results. This surface can be divided into three parts.

(a) Holes in the first band centered at or near $K$ and $U$ [Figs. 6(a) and 6(b)] which are *very* sensitive to the exact position of the Fermi level. In fact, from our calculation these pieces are actually ⟨110⟩ arms connecting the holes at $W$ discussed below, but only minor changes in the potential would be required to break this connection.

(b) First-band holes centered at $W$ [Fig. 6(c)].

(c) Second-band electron pockets centered at $L$ [Fig. 6(d)].

This surface is similar to those obtained from several other calculations. The main differences

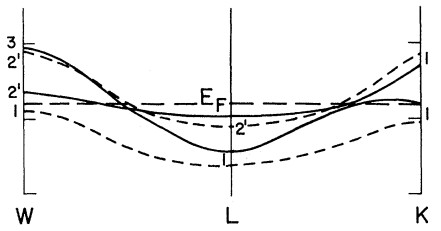


FIG. 7. Two lowest energy bands of Ca at normal lattice constant along the $W$-$L$-$K$ directions. The solid lines are the APW bands while the dashed lines are the four-OPW bands.

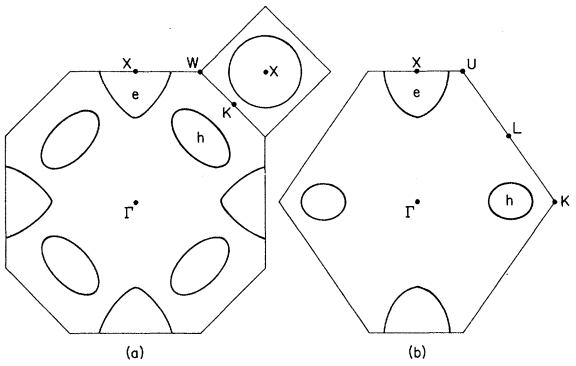


FIG. 8. Cross sections of the Fermi surface of Ca at a reduced lattice spacing of $a/a_0 = 0.7$.

seem to result from the uncertainty in the position of the Fermi level. Chatterjee and Chakraborti[6] found holes at $K(U)$ and electrons at $L$ and just missed having holes at $W$. (In the quantum-defect calculation[8] holes at $W$ were found.)

Vasvari[21] chose his Fermi energy to obtain a "best fit" to de Haas–van Alphen (dHvA) measurements and obtained a "dismembered nearly-free-electron *monster*" with hole pockets at $W$ and electron pockets at $L$. Altmann *et al.*[9] have pointed out that Vasvari's surface did not seem to have the required equality of hole and electron volumes. Moreover, Altmann *et al.* obtained qualitatively the same Fermi surface as we did and suggested that such a surface, including the first-band connected hole regions, could satisfactorily explain the dHvA

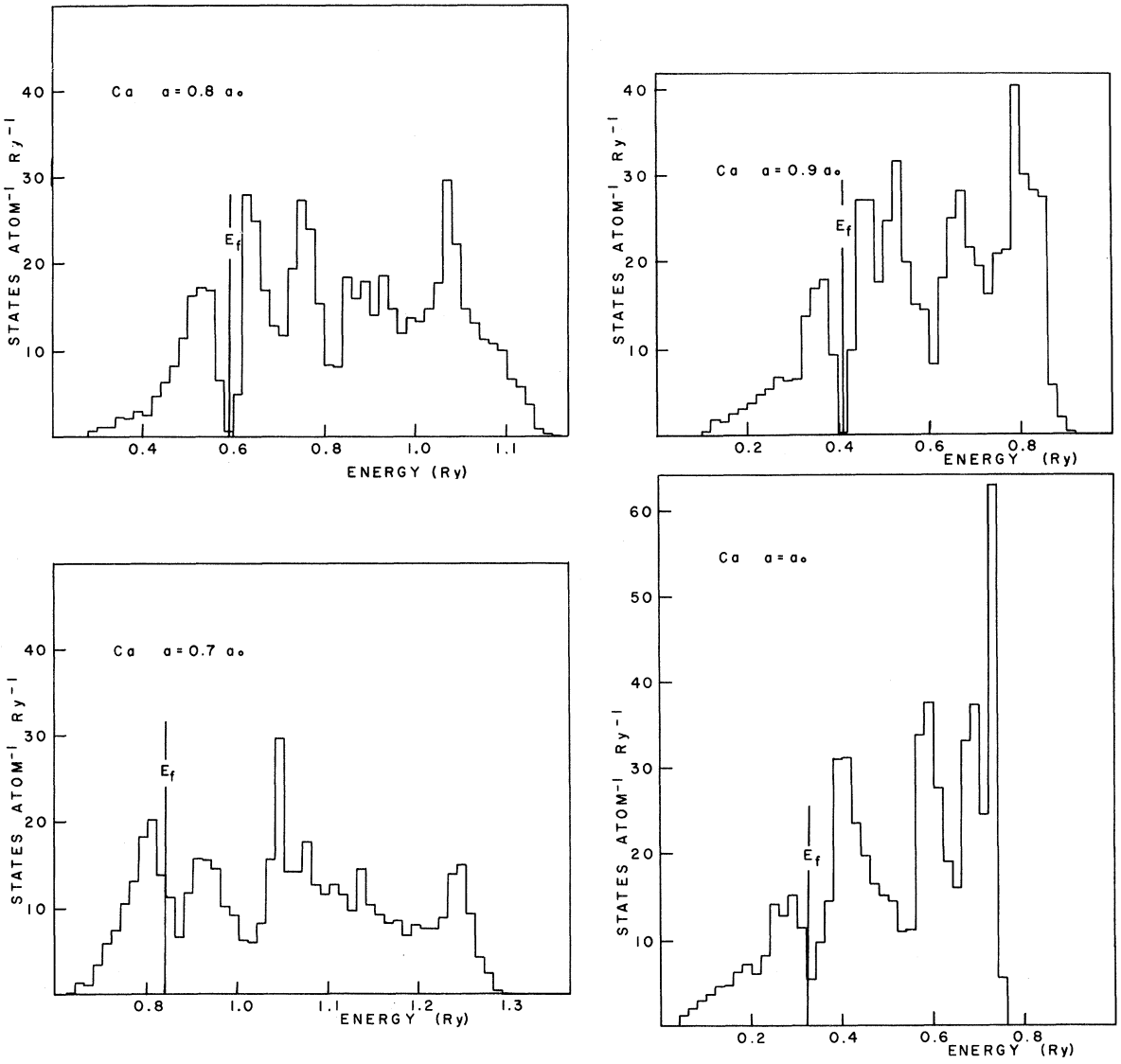


FIG. 9. Variation of the density of states of Ca with lattice constant.

TABLE II. Experimental and calculated Fermi surface at normal lattice spacing.

| Orbit nomenclature | Direction | Area [Units of $(2\pi/a)^2$] Calculated APW | Calculated Cellular[a] | Experimental | dHvA period[b] ($10^{-7}$ G$^{-1}$) |
|---|---|---|---|---|---|
| $\zeta$ | [110] | 0.009 | 0.020 | 0.0246 | 3.05($\gamma$) |
| $\nu_1$ | [100] | 0.12 | | 0.0975 | 0.77($\alpha$) |
| $\nu_2$ | [110] | 0.15 | | 0.132 | 0.57($\beta$) |
| $\nu_3$ | near [100] | | 0.13 | | |
| $\lambda_1$ | [110] | 0.05 | 0.11 | | |
| $\lambda_2$ | [111] | 0.41 | 0.49 | | |
| $\theta$ | [111] | 0.72 | 0.66 | | |
| $\xi$ | [100] | 0.32 | 0.37 | | |
| $\mu$ | [100] | 0.77 | 0.86 | | |

[a]Altmann *et al.* (Ref. 9). [b]Condon and Marcus (Ref. 28). The Greek letters refer to labeling of the periods in the text.

results.

Condon and Marcus[28] found three dominant dHvA periods, $P_\alpha = 0.77 \times 10^{-7}$ G$^{-1}$, $P_\beta = 0.57 \times 10^{-7}$ G$^{-1}$, and $P_\gamma = 3.05 \times 10^{-7}$ G$^{-1}$ in their work on calcium (see Table II). Unfortunately, since they worked with polycrystalline samples, it is not possible to be certain of the crystal directions corresponding to their dHvA measurements. In spite of this, Condon and Marcus found it plausible to associate $P_\alpha$ and $P_\gamma$ with ⟨110⟩ directions and $P_\beta$ with orientations near ⟨100⟩. In Table II our calculated extremal cross sections are compared with the dHvA data and with the values calculated by Altmann *et al.* For this comparison, we have assumed that $P_\beta$ actually corresponds to ⟨100⟩ orientations.

The orbit nomenclature, except for $\nu_2$, is shown in Fig. 6. The $\zeta$ orbits result from a (110) first-band cross section containing $K$(or $U$), whereas the $\nu$ orbits are obtained from the holes at $W$. In particular, if the coordinates at $W$ are ($\frac{1}{2}$, 0, 1), then $\nu_1$ and $\nu_2$ correspond to cross sections containing $W$ and perpendicular to the [100] and [011] directions, respectively.

We have assumed that $P_\gamma$ results from $\zeta$, $P_\alpha$ from $\nu_1$, and $P_\beta$ from $\nu_2$. There is rather good agreement with dHvA periods for the $\nu_1$ and $\nu_2$ orbits, but the calculated $\zeta$ cross section is more than a factor of 2 too small. This discrepancy is probably not significant, since small changes in the potential could appreciably increase this small area.

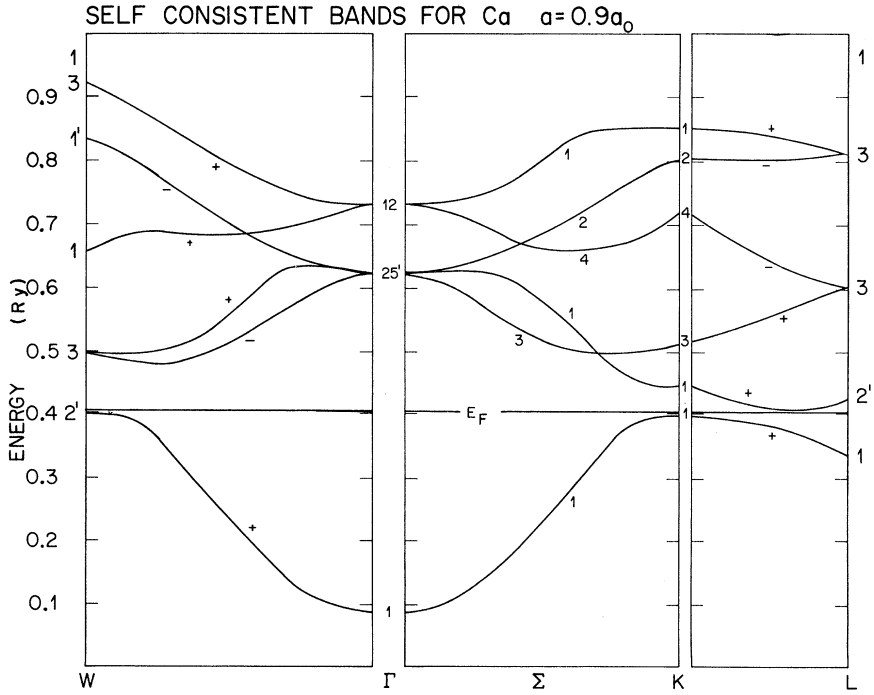


FIG. 10. Energy bands of Ca for $a/a_0 = 0.9$ along the $W$-$\Gamma$-$K$-$L$ symmetry directions.

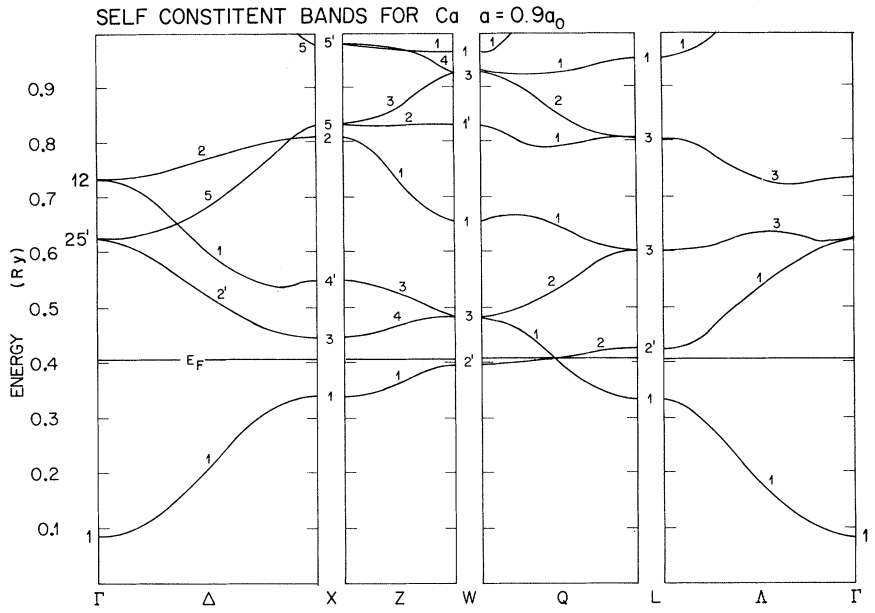


FIG. 11. Energy bands of Ca for $a/a_0 = 0.9$ along the $\Gamma$-$X$-$W$-$L$-$\Gamma$ symmetry directions.

Altmann *et al.* have assumed instead that the $P_\beta$ period results from the electron pockets at $L$, that is a $\lambda_1$-type orbit. However, from our calculations, even with allowance for slight modifications of the potential, it does not appear to be possible to obtain a $\lambda_1$ cross-sectional area that is large enough and still retain the agreement with dHvA data for the $\zeta$ and $\nu_1$ orbits. The other cross sections in Table II, $\lambda_2$, $\theta$, $\xi$, and $\eta$ are of much larger area and probably could not have been observed in the samples used by Condon and Marcus. Verification of the details of any calculated Fermi surface will require dHvA measurements on single crystals.

In order to exhibit the limitations of an interpolation model which neglects the $d$-band contribution, we have determined two Fourier components of a local pseudopotential, $V_{111}$ and $V_{200}$. These Fourier coefficients have been obtained as parameters from a fit to the APW bands near the Fermi surface. The method used in fitting was the four-OPW pseudopotential interpolation scheme which proved successful for aluminum.[29–31] The two parameters, $V_{111}$

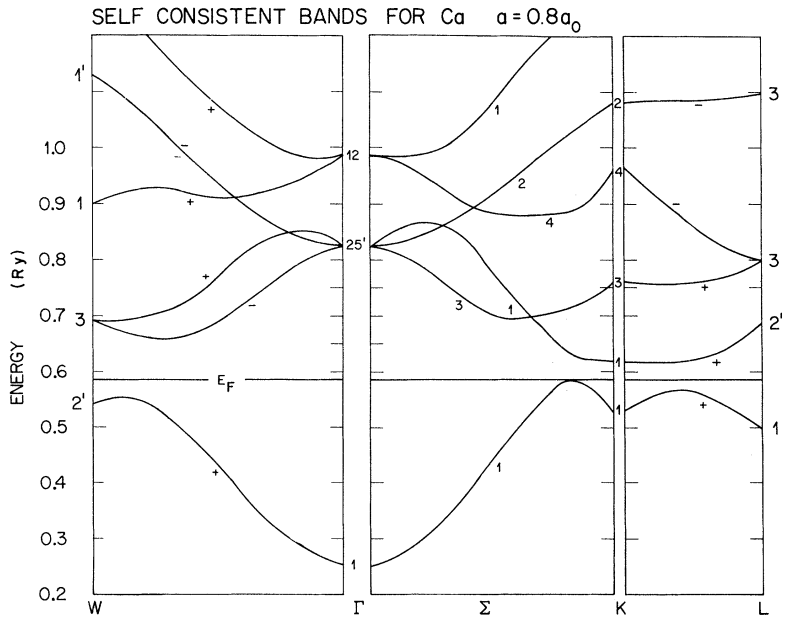


FIG. 12. Energy bands of Ca for $a/a_0 = 0.8$ along the $W$-$\Gamma$-$K$-$L$ symmetry directions.

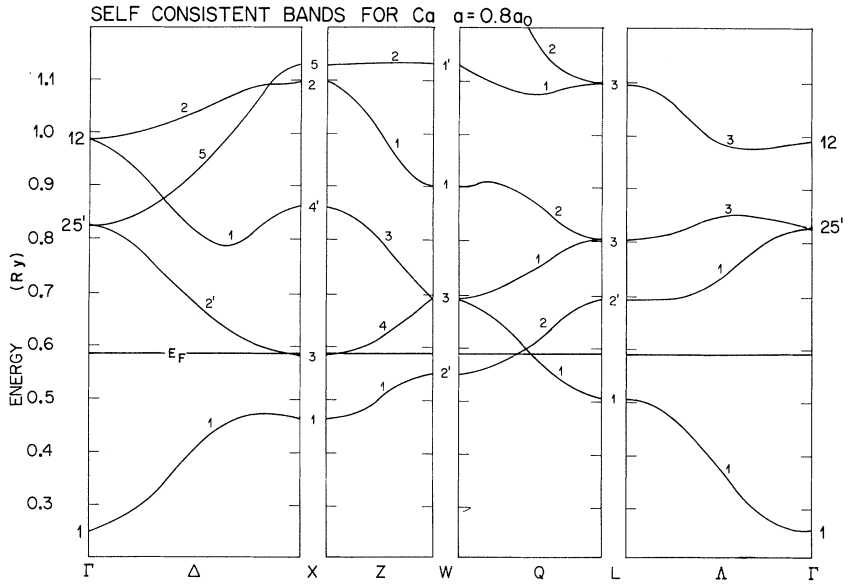


FIG. 13. Energy bands of Ca for $a/a_0 = 0.8$ along the $\Gamma$-$X$-$W$-$L$-$\Gamma$ symmetry directions.

and $V_{200}$, were obtained from the three APW eigenvalues nearest the Fermi energy corresponding to the symmetries $K_1$, $L_1$, and $X_1$. By minimizing the squares of the differences between the four-OPW energies and the APW energies, the values $V_{111} = -0.021$ Ry and $V_{200} = -0.098$ Ry were obtained. We note that these values do not agree with the predictions of the Heine–Abarenkov model potential,[32,33] since both $V_{111}$ and $V_{200}$ are negative and the magnitude of $V_{200}$ is greater than that of $V_{111}$.

In Fig. 7, $E(\vec{k})$ curves determined by both the APW and four-OPW methods are compared. It is obvious that the two calculations are not similar even near the Fermi energy. For example, the two lowest four-OPW bands between $L$ and $W$ do not cross, in contradiction to the APW bands. With the four-OPW bands, calcium could become a semiconductor at high pressures. In addition, the band ordering at $W$ is changed since the lowest four-OPW level is $W_1$ rather than $W_2'$. Since we have also tried other combinations of $V_{111}$ and $V_{200}$ without success, we must conclude that a simple local interpolation approach which ignores the effects of the $d$ bands is not applicable to calcium even in describing only the Fermi surface. An attempt was also made to use the composite interpolation scheme of Hodges

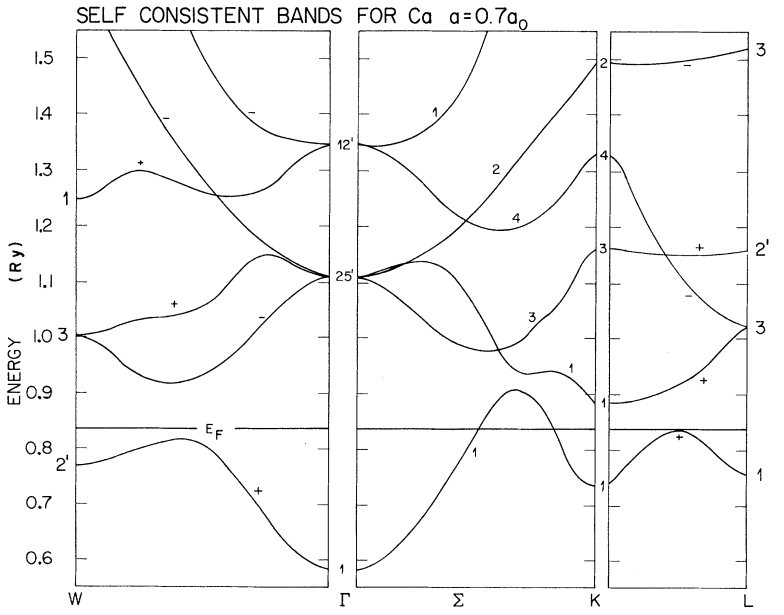


FIG. 14. Energy bands of Ca for $a/a_0 = 0.7$ along the $W$-$\Gamma$-$K$-$L$ symmetry directions.

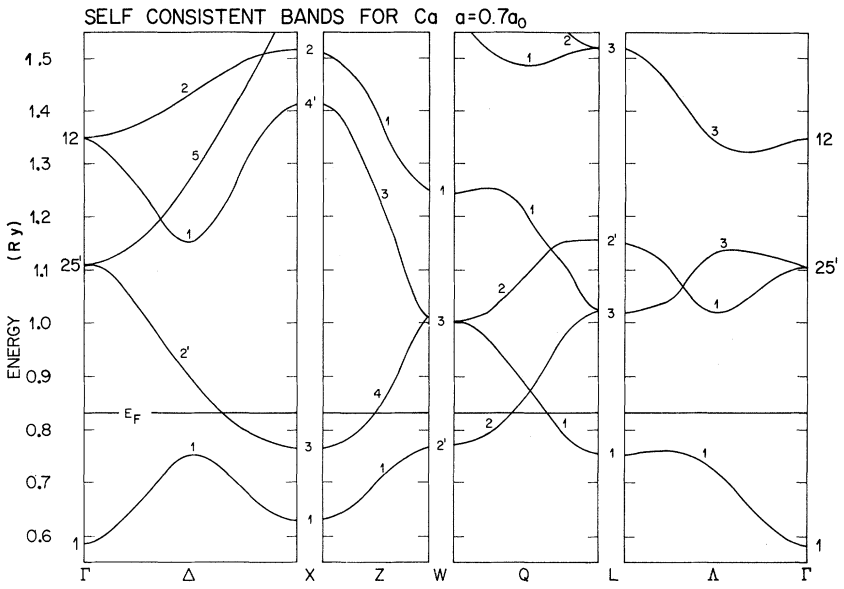


FIG. 15. Energy bands of Ca for $a/a_0 = 0.7$ along the $\Gamma$-$X$-$W$-$L$-$\Gamma$ symmetry directions.

and Ehrenreich[34] to fit the APW results, but the hybridization parameters $B_1$ and $B_2$ appeared to be unphysical. This approach merits further study. On the other hand, Vasvari,[21] using a nonlocal model potential, obtained both the crossing between $W$ and $L$ and the same ordering of the bands at $W$ as we found with the APW method.

TABLE III. $l$ character of band-state charge of Ca for $\alpha = \frac{2}{3}$.

| State | $a/a_0$ | $Q_{out}$ | $Q_s$ | $Q_p$ | $Q_d$ | $Q_f$ |
|---|---|---|---|---|---|---|
| $\Gamma_1$ | 1.0 | 0.305 | 0.695 | 0 | 0 | 0 |
| | 0.9 | 0.324 | 0.676 | 0 | 0 | 0 |
| | 0.8 | 0.352 | 0.648 | 0 | 0 | 0 |
| | 0.7 | 0.375 | 0.624 | 0 | 0 | 0 |
| $\Delta_1(040)$ | 1.0 | 0.309 | 0.499 | 0.165 | 0.027 | 0 |
| | 0.9 | 0.326 | 0.467 | 0.164 | 0.042 | 0 |
| | 0.8 | 0.348 | 0.412 | 0.160 | 0.079 | 0 |
| | 0.7 | 0.622 | 0.033 | 0.084 | 0.147 | 0 |
| $X_1(080)$ | 1.0 | 0.314 | 0.158 | 0 | 0.526 | 0 |
| | 0.9 | 0.305 | 0.114 | 0 | 0.580 | 0 |
| | 0.8 | 0.316 | 0.085 | 0 | 0.597 | 0 |
| | 0.7 | 0.326 | 0.065 | 0 | 0.606 | 0 |
| $\Sigma_1(444)$ | 1.0 | 0.307 | 0.334 | 0.276 | 0.081 | 0.002 |
| | 0.9 | 0.317 | 0.298 | 0.273 | 0.108 | 0.026 |
| | 0.8 | 0.328 | 0.255 | 0.267 | 0.145 | 0.004 |
| | 0.7 | 0.308 | 0.211 | 0.251 | 0.222 | 0.005 |
| $L_1(444)$ | 1.0 | 0.218 | 0.416 | 0 | 0.368 | 0 |
| | 0.9 | 0.216 | 0.335 | 0 | 0.447 | 0 |
| | 0.8 | 0.220 | 0.268 | 0 | 0.511 | 0 |
| | 0.7 | 0.218 | 0.210 | 0 | 0.570 | 0 |
| $L_2'(444)$ | 1.0 | 0.374 | 0 | 0.611 | | 0.015 |
| $W_2'(480)$ | 0.9 | 0.318 | 0 | 0.126 | 0.543 | 0.012 |
| | 0.8 | 0.321 | 0 | 0.110 | 0.554 | 0.013 |
| $X_3(080)$ | 0.7 | 0.174 | 0 | 0 | 0.822 | 0 |

We have also determined the APW Fermi surface at a reduced lattice spacing of $a/a_0 = 0.7$ (Fig. 8). In this case there are only two pieces of Fermi surface; electron pockets at $X$ and hole pockets near $K$. The changes in the Fermi surface occur because $X_3$ drops below $E_F$ while $W_2'$ and $L_2'$ rise above $E_F$ as the lattice constant decreases. Because it is unlikely that there will be experiments probing the details of the Fermi surface at such reduced lattice spacings, we are not presenting additional details of the changes of Fermi surface with pressure in this report.

## V. DENSITY OF STATES AT NORMAL AND REDUCED LATTICE SPACING

The electron density of states of Ca $N(E)$ at normal and reduced lattice spacing was calculated by interpolating the energy-band results to 48 000 points in the zone using a Monte-Carlo method. This is shown in Fig. 9.

The results clearly demonstrate metallic behavior for $a/a_0 = 1[N(E_F) = 11.1$ states atom$^{-1}$ Ry$^{-1}]$. However, for $a/a_0 = 0.9$ there is a "cusp" in the density of states at the Fermi energy and $N(E_F)$ is zero. This corresponds to a "zero-gap" semiconductor. At $a/a_0 = 0.8$ a pronounced dip in the density of states remains and the density of states at the Fermi energy is still very small, while for $a/a_0 = 0.7$ there is again metallic behavior and $N(E_F) = 12$ states atom$^{-1}$ Ry$^{-1}$.

From the density of states at the Fermi energy we calculated the temperature coefficient of the electronic specific heat $\gamma$ at normal lattice spacing and found a value of 1.94 mJ °K$^{-2}$ mole$^{-1}$. This

is to be compared with an experimental value of 2.9 mJ $°K^{-2}$ $mole^{-1}$.[35] If we attribute that discrepancy to the electron-phonon interactions, this would correspond to an enhancement factor of 1.5. A model-potential calculation,[36] which did not directly treat $d$ bands, gave an enhancement factor of only 1.28 for Ca.

It should also be pointed out that Williams and Davies[37] have calculated $\gamma$ as a function of exchange factor $\alpha$; however, they ignored the electron-phonon enhancement which we have found to be fairly large.

ACKNOWLEDGMENTS

We are indebted to A. C. Switendick for helpful discussions and computer programs. The support of the University of Maryland Computer Science Center is gratefully acknowledged.

APPENDIX

The self-consistent energy bands of calcium for reduced lattice spacings of 0.9, 0.8, and 0.7 are given in Figs. 10 and 11, 12 and 13, and 14 and 15, respectively.

The $l$ character of the band state charge of Ca is given in Table III.

---

*Work supported in part by the Advanced Research Projects Agency.

†Work supported in part by the National Science Foundation.

[1]J. W. McCaffrey, D. A. Papaconstantopoulos, and J. R. Anderson, Solid State Commun. 8, 2109 (1970).

[2]R. A. Stager and H. G. Drickamer, Phys. Rev. 131, 2524 (1963).

[3]A. A. Bakanov and I. P. Dudoladov, Zh. Eksperim. i Teor. Fiz. Pis'ma v Redaktsiyu 5, 322 (1967) [JETP Letters 5, 265 (1967)].

[4]L. F. Vereshchagin, A. A. Semerchan, and N. N. Kuzin, Dokl. Akad. Nauk SSSR 186, 1045 (1969) [Sov. Phys. Doklady 14, 557 (1969)].

[5]J. A. Dreesen and L. Pyenson, Phys. Rev. B 2, 4852 (1970).

[6]S. Chatterjee and D. K. Chakraborti, J. Phys. C Suppl. 3, S120 (1970).

[7]M. Ross and K. Johnson, J. Phys. F 1, L13 (1971).

[8]S. Chatterjee and D. K. Chakraborti, J. Phys. F 1, 638 (1971).

[9]S. L. Altmann, A. R. Harford, and R. G. Blake, J. Phys. F 1, 791 (1971).

[10]K. A. Kress and G. J. Lapeyre, Solid State Commun. 9, 827 (1971).

[11]L. F. Mattheiss, J. H. Wood, and A. C. Switendick, in *Methods in Computational Physics* 8, edited by B. Alder, S. Fernbach, and M. Rotenberg (Academic, New York, 1968).

[12]T. Loucks, *Augmented Plane Wave Method* (Benjamin, New York, 1967).

[13]J. O. Dimmock, Solid State Phys. 26, 103 (1971).

[14]F. Herman and S. Skillman, *Atomic Structure Calculations* (Prentice-Hall, Englewood Cliffs, N. J., 1963).

[15]P. O. Löwdin, Advan. Phys. 5, 1 (1965).

[16]W. B. Pearson, *A Handbook of Lattice Spacing and Structures of Metals and Alloys* (Pergamon, London, 1967), Vol. 2, p. 81.

[17]J. C. Slater, Phys. Rev. 81, 385 (1951).

[18]R. Gaspar, Acta Phys. Acad. Sci. Hung. 3, 263 (1954); W. Kohn and L. J. Sham, Phys. Rev. 140, A1133 (1965).

[19]R. H. Kingston, Phys. Rev. 84, 944 (1951).

[20]L. D. Finkelshteyn and S. A. Nemnonov, Fiz. Metal. i Metalloved. 22, 843 (1966) [Phys. Metals Metallog. 38, 38 (1969)].

[21]B. Vasvari, A. O. E. Animalu, and V. Heine, Phys. Rev. 154, 535 (1967); B. Vasvari, Rev. Mod. Phys. 40, 776 (1968).

[22]J. Korringa, Physica 13, 392 (1947); W. Kohn and N. Rostoker, Phys. Rev. 94, 1411 (1954).

[23]D. Liberman, Phys. Rev. 171, 1 (1968).

[24]E. Kmetko, Phys. Rev. A 1, 37 (1970).

[25]G. Johansen and A. R. Mackintosh, Solid State Commun. 8, 121 (1970).

[26]D. B. McWhan, T. M. Rice, and P. M. Schmidt, Phys. Rev. 177, 1063 (1969).

[27]D. Jerome and M. Rieux, Solid State Commun. 7, 957 (1969).

[28]J. H. Condon and J. A. Marcus, Phys. Rev. 134, A466 (1964).

[29]W. A. Harrison, *Pseudopotentials in the Theory of Metals* (Benjamin, New York, 1966), pp. 100–116.

[30]N. W. Ashcroft, Phil. Mag. 8, 2055 (1963).

[31]J. R. Anderson and S. S. Lane, Phys. Rev. B 2, 298 (1970).

[32]V. Heine and I. Abarenkov, Phil. Mag. 9, 451 (1964).

[33]I. Abarenkov and V. Heine, Phil. Mag. 12, 529 (1965).

[34]L. Hodges and H. Ehrenreich, in Ref. 11.

[35]L. M. Roberts, Proc. Phys. Soc. (London) B70, 738 (1957).

[36]A. O. E. Animalu and V. Heine, Phil. Mag. 12, 1249 (1965).

[37]R. W. Williams and H. L. Davies, in *Electronic Density of States*, edited by L. M. Bennett (U. S. GPO, Washington, D.C., 1971), p. 57.